ChemComm

Accepted Manuscript

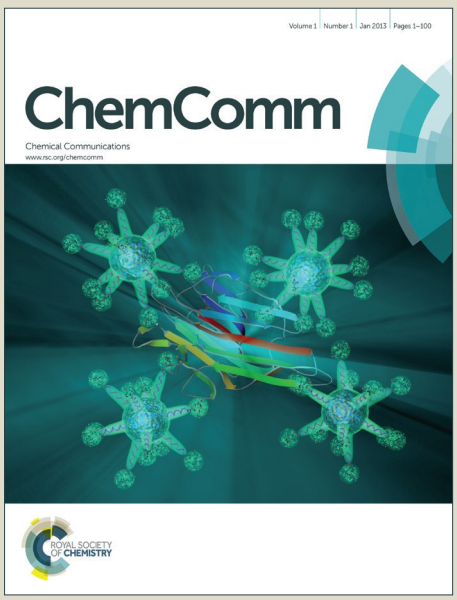

ROYAL SOCIETY OF CHEMISTRY

www.rsc.org/chemcomm

Cite this: DOI: 10.1039/c0xx00000x

www.rsc.org/xxxxxx

ARTICLE TYPE

Anion-Induced Palladium Nanoparticle Formation During the On-Surface Growth of Molecular Assemblies

Michael Morozov,[†] Tatyana Bendikov,[‡] Guennadi Evmenenko,[§] Pulak Dutta,[§] Michal Lahav,[†] Milko E. van der Boom[†,*]

Received (in XXX, XXX) Xth XXXXXXXXX 20XX, Accepted Xth XXXXXXXXX 20XX
DOI: 10.1039/b000000x

We demonstrate a process that results in the formation of palladium nanoparticles during the assembly of molecular thin films. These nanoparticles are embedded in the films and are generated by a chemical reaction of the counter anions of the molecular components with the metal salt that is used for cross-linking these components.

Anions are known to control the structures and functions of complex and large coordination-based structures including molecular cages.[1] The importance of the role that anions play in numerous supramolecular processes cannot be overstated.[2-4] In most cases, the anions play a structural stabilizing role and do not undergo chemical transformations.

The stepwise assembly of coordination-based polymers from solution on solid interfaces has opened up many possibilities to systematically study and control their properties.[5-7] These materials are being studied for their properties in relation to electron transfer,[8-12] electrochromics,[12-15] solar cells,[16] and Boolean logic,[17-18] among others.[19-21] Nishihara,[9] and others have reported structural factors that affect the electrochemical and the electron transport properties of surface-bound metallo-organic oligomers.[8-12, 21] The formation of such materials often includes the build-up of metal complexes during the assembly procedure,[22-24] or the use of structurally defined complexes that are being integrated into larger structures.[22] We have reported that the alternative deposition of polypyridyl complexes of cobalt, iron, ruthenium, osmium, as well as palladium dichloride from solution results in linear and exponentially growing molecular assemblies.[25-26] The overall reaction is essentially a three-component process in which the self-propagating molecular assemblies (SPMAs) store excess of the d^8 palladium salt. The palladium salt is used to coordinatively bind polypyridyl complexes from solution to the surface of the assembly.[25]

We introduce here an assembly process that generates coordination-based molecular materials with the concurrent formation of embedded metallic nanoparticles. This new process is demonstrated by the formation of composite materials consisting of redox-active ruthenium complexes (**1•BPh$_4$**) and palladium nanoparticles (PdNPs) (Scheme 1). Pre-synthesized NPs have been embedded in thin films from solution using Layer-by-Layer (LbL) deposition and other methods.[27-32] Immobilization of metal complexes in polymers followed by a reduction process has been used as well.[30] In our method, PdNPs are generated *in-situ* by a redox reaction between the tetraphenylborate anions (BPh_4^-) of the ruthenium complexes and an excess of palladium(II) present in the films. Tetraphenylborate is known to reduce palladium(II).[33]

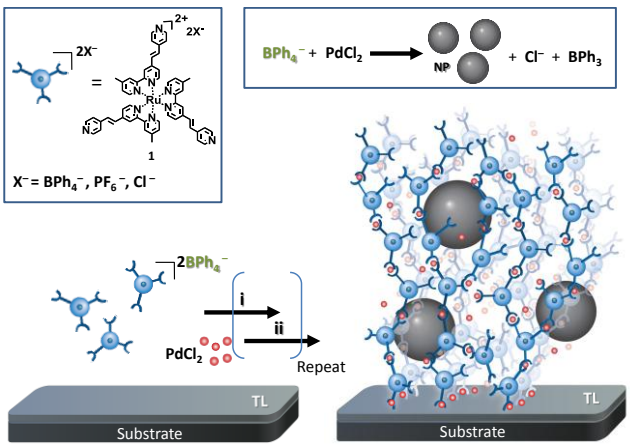

Scheme 1. Schematic representation of the formation of self-propagating molecular assemblies (SPMAs) by alternating deposition of a Pd salt and complex **1** upon a pyridine-terminated template layer (**TL**) (Figs. S1-2, ESI†).[34] For **1•BPh$_4$**: the anion reduces the Pd(II) to form nanoparticles.

The new PdNP-containing SPMAs were formed by using a step-wise assembly procedure. Quartz, silicon, and indium-tin-oxide (ITO)-coated glass substrates were functionalized with an template layer (TL)[34] having pyridine groups available for coordination to palladium (Fig. S2, ESI†). Subsequently, twelve iterative 15 min immersions of these substrates into a THF solution of $PdCl_2(PhCN)_2$ (1.0 mM) and a THF/DMF (3:7 v/v; 0.2 mM) solution of complex **1•BPh$_4$** resulted in the formation of the SPMAs. The films were washed and sonicated (3 × 3 min.) in organic solvents between the deposition steps. The SPMAs have been characterized by combining several complementary analytical methods: optical (UV/Vis and ellipsometry)

spectroscopy, synchrotron X-ray reflectivity (XRR), X-ray photoelectron spectroscopy (XPS), scanning electron microscopy (SEM), Atomic Force Microscopy (AFM) and electrochemistry. For comparison, we generated also an SPMA with complex **1•PF$_6$**.

The UV/Vis measurements indicated a near-linear growth for **1•BPh$_4$** and exponential growth for **1•PF$_6$**. For both SPMAs, a good correlation was observed between the number of depositions of the polypyridyl complexes, and the intensity of the ligand $\pi \rightarrow \pi^*$ and the metal-to-ligand-charge transfer (MLCT) absorption bands at λ = 316 nm and λ = 500 nm, respectively (Figs. 1A, S3, ESI†). The noticable difference (3×) in the increase in the optical absorption for **1•BPh$_4$** and **1•PF$_6$** (Fig. 1A, inset). can be attributed to the reduction of Pd(II) by $[BPh_4]^-$ and the subsequent formation of NPs (*vide infra*). Therefore, less $PdCl_2$ is available for binding of additional complexes of **1•BPh$_4$** to the assembly resulting in near-linear growth. The linear versus exponential growth for SPMAs is a function of the available metal salt.[25-26] The film thicknesses obtained by ellipsometry showed also a near-linear growth for **1•BPh$_4$** and exponential growth for **1•PF$_6$**. (Fig. 1B). The linear dependence between the absorption intensities and the thicknesses indicates that the structural regularity was maintained during the growth (Fig. S9, ESI†). The molecular densities for both SPMAs are very similar: 0.8 molecules/nm^3 (**1•BPh$_4$**) and 1.0 molecules/nm^3 (**1•PF$_6$**). We also build-up an SPMA by twelve alternating depositions of **1•BPh$_4$** and **1•PF$_6$**, starting with the deposition of **1•PF$_6$**. Interestingly, the UV/Vis and ellipsometry data show that the growth of this SPMA follows the same trend observed for the SPMA formed from **1•PF$_6$** (Fig. S4, ESI†). Apparently, the presence of **1•PF$_6$** in each alternating layer is sufficient to maximize the film growth. A similar observation has been reported when using layers of two different molecular buildings block in one assembly.[34] The layers consisting of polypyridyl complexes induced exponential growth in layers of organic chromophores.

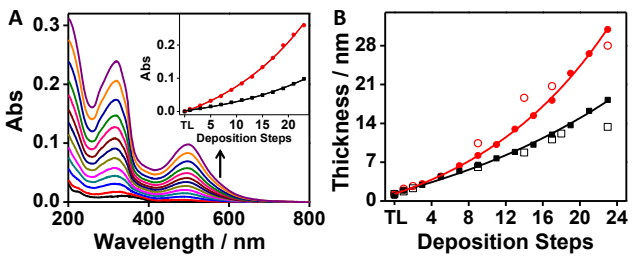

Fig. 1 (A) UV/Vis absorption data of self-propagating molecular assemblies (SPMAs) for 12 depositions of **1•BPh$_4$**. Inset: absorption intensities of the MLCT band (λ = 500 nm) versus the number of **1•BPh$_4$** (black) or **1•PF$_6$** (red) deposition steps. (B) SPMA thickness versus the number of **1•BPh$_4$** (black) or **1•PF$_6$** (red) deposition steps. Closed symbols = ellipsometry and open symbols = X-ray reflectivity. $R^2 \geq 0.998$ for all fits. TL refers to the template layer (Fig. S2, ESI†).[34]

Selected samples of SPMAs, generated from **1•BPh$_4$** or **1•PF$_6$**, were analyzed by synchrotron X-ray reflectivity measurements (XRR),[35] confirming the film thicknesses observed by ellipsometry (Figs. 1B, 2, S5, ESI†). Interestingly, the electron density and roughness (ρ = 0.53 e·Å^{-3}; $R \approx$ 9 Å) are similar for both SPMAs and remained constant throughout their formation (Fig. 2), thus indicating homogeneous structures. A dendritic divergent growth is unlikely to exhibit such an electron density profile.[36] AFM measurements of SPMAs having a thickness of 12 nm indicated that they share similar surface morphologies with $R_{rms} \approx$ 0.5 nm, and exhibit areas having depths of 1.5-3.0 nm and widths of 10-35 nm.

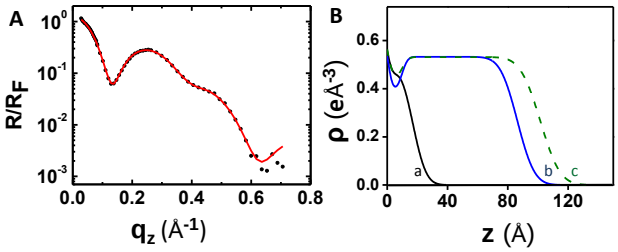

Fig. 2 (A) Representative synchrotron X-ray reflectivity (XRR) data: self-propagating molecular assemblies (SPMAs) formed from **1•BPh$_4$** (6.1 nm; roughness 8.4 Å) on a silicon substrate in which R is the reflectivity normalized to the Fresnel reflectivity R_F. The red trace is a fit to the experimental data.[35] (B) XRR-derived electron density profiles for the template layer (TL; solid line a; Fig. S2, ESI†), SPMAs formed from **1•BPh$_4$** [solid line, b (8.7 nm)] and from **1•PF$_6$** [dashed line, c (10.5 nm)]. The minima around 0.8 nm represents the TL (a)[34] and the plateaus correlates to the SPMAs.

Scanning electron microscopy (SEM) analysis of those SPMAs having a thickness of 12 nm revealed the formation of NPs only with **1•BPh$_4$**. These NPs have an average diameter of ~12.5 nm (Fig. 3A). High-resolution XPS spectra acquisition revealed the presence of significant amounts (20%) of Pd(0) in the SPMAs generated with **1•BPh$_4$** (Fig. 3B; $E_B(Pd_{5/2}) \approx$ 335 eV).[37] Metal centers are known to undergo reduction during the measurements; however, the amount of Pd(0) remained constant during the measurements. Therefore, the observed Pd(0) is the result of a reduction reaction with the surface-bound **1•BPh$_4$** and $PdCl_2(PhCN)_2$. These findings are in good agreement with the SEM data and the expected reactivity of **1•BPh$_4$** and **1•PF$_6$** with the palladium salt. Although similar amounts of excess Pd(II) are observed by XPS for both SPMAs (Pd/Ru ≈ 3 at 0° takeoff angle; $E_B(Pd_{5/2}) \approx$ 338 eV),[37] the growth with **1•BPh$_4$** is less efficient, which may be explained by the trapping of some of the Pd(II) by the NPs. The theoretical Pd/Ru ratio is 1.5 for a saturated network with all the vinylpyridines of **1•BPh$_4$** or **1•PF$_6$** cross-linked with palladium. To confirm the reactivity of $[BPh_4]^-$ with $PdCl_2$, both model complexes $Ru(bpy)_3(PF_6)_2$ and $Ru(bpy)_3(BPh_4)_2$ were reacted with $PdCl_2PhCN_2$ in solution to evaluate their reactivity and structural stability. Mixing $Ru(bpy)_3(BPh_4)_2$ with $PdCl_2PhCN_2$ resulted in electron-transfer, as judged by the formation of colloidal palladium and a change in the solution's color from orange to brown (Figs 3B inset, S6, ESI†). The formation of triphenylborane (BPh_3) was observed by $^{11}B\{^1H\}$ NMR, which showed a singlet resonance at δ 45 ppm.[38-39] UV/Vis spectrometry and mass spectrometry indicated that the molecular structure of the $Ru(bpy)_3$ remained intact with chloride as counter anions. XPS measurements of the black participate revealed the formation of Pd(0). As expected, no reduction of Pd(II) was observed when $Ru(bpy)_3(PF_6)_2$ was used.

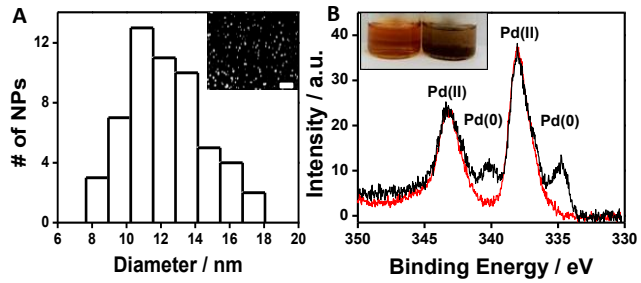

Fig. 3 (A) The size distribution of palladium NPs of self-propagating molecular assemblies (SPMAs) formed from **1•BPh$_4$** (12 nm). Inset: Scanning Electron Microscopy (SEM) image. The white scale bar = 100 nm. (B) Normalized X-ray photoelectron spectroscopy (XPS) spectra of the Pd 3d region for SPMAs (10 nm) formed from **1•BPh$_4$** (black line) and from **1•PF$_6$** (red line).[37] The samples were measured at a takeoff angle of 0°. Inset: Photographs showing glass vials of the reaction of $PdCl_2(PhCN)_2$ with $Ru(bpy)_3(PF_6)_2$ (left) or $Ru(bpy)_3(BPh_4)_2$ (right) (Fig. S6, ESI†). For (A) and (B), silicon substrates were used.

Cyclic voltammetry measurements showed that SPMAs with thicknesses of 7 nm and 12 nm exhibit well-defined surface waves characteristic of the $Ru^{2+/3+}$ couple on ITO with a half-wave redox potential, $E_{½}$, at about 1.2 V versus Ag/Ag+ (with ferrocene as an internal reference, $E_{½}$ = 0.40 V) (Fig. 4A, S7, ESI†). The $E_{½}$ value was not affected by the differences in thickness and the presence of the palladium NPs. The permeability of the two SPMAs (7 nm thickness) was evaluated using two electrochemically active probes having different volumes (estimated by DFT): 2,6-dimethoxy-1,4-benzoquinone (228 Å^3) and 3,3',5,5'-tetra-tretbutyldiphenylphenoquinone (640 Å^3) (Fig. 4B, S8, ESI†). The SPMA generated with **1•BPh$_4$** is slightly more porous than is the SPMA formed from **1•PF$_6$** as indicated by the difference in the anodic and cathodic peak currents, i_{pa} and i_{pc}. Our observations are in good agreement with our previous mechanistic studies showing that the SPMAs are porous structures capable of storing and using metal salts for their growth.[25-26, 35, 40]

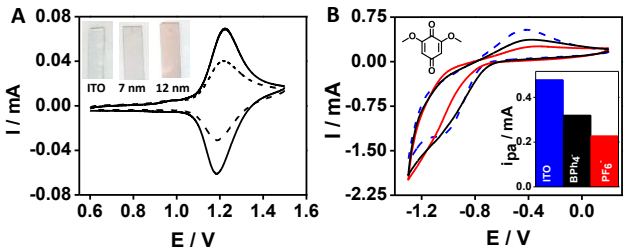

Fig. 4 (A) Representative cyclic voltammograms (CVs) of self-propagating molecular assemblies (SPMAs) formed from **1•BPh$_4$** (7 nm, dotted line; 12 nm, solid line) recorded on single-sided ITO-coated glass. Inset: photographs of the electrodes (0.7 cm × 2 cm). (B) Representative CVs of 2,6-dimethoxy-1,4-benzoquinone (1.3 mM, CH_3CN) for a double-sided ITO electrode (blue line), and the same electrodes coated with SPMAs formed from **1•BPh$_4$** (7 nm, black line) and from **1•PF$_6$** (7 nm; red line). Inset: bar diagram showing the differences in the anodic peak currents (i_{pa}) for the three systems. The experiments were carried out at rt under argon in 0.1 M ^{n}Bu$_4$NPF$_6$/CH_3CN at a scan rate of 100 mVs^{-1}. The ITO-coated glass, Pt wire and Ag/Ag$^+$ were used as working, counter, and reference electrodes, respectively.

Conclusions

The counter anions of cationic metal complexes can be used to generate composite assemblies by redox chemistry. The deposition steps in the here-presented assembly do not just add materials to the surface; they enforce multiple transformations including the formation of nanoparticles. Overall, the structure and properties of such assemblies, consisting of both molecular components and metallic NPs, very much resemble those of assemblies lacking the NPs. However, less material is being deposited for the NP containing assembly. Besides the presence of the NPs, large structural differences between the supramolecular structures are not apparent from the optical, XRR and electrochemical data, including the permeability of the assemblies by organic molecules. The molecular density is nearly identical regardless of the presence of metallic NPs. Significant differences were found in the growth of the assemblies; the assemblies with the NPs grow slower. The *in-situ* generation of NPs by and from the different building blocks and their subsequent integration into the assemblies can be considered a new route towards the formation of functional coatings with a high degree of structural complexity.

Acknowledgments

This research was supported by the Helen and Martin Kimmel Center for Molecular Design, the Israel Science Foundation (289/09), MINERVA, Use of the Advanced Photon Source was supported by the U.S. Department of Energy, Office of Science, Office of Basic Energy Sciences, under Contract No. DE-AC02-06CH11357. GE and PD were supported by the U.S. National Foundation under Grant No. DMR-1309589. GE gratefully acknowledge support from the Center for Electrochemical Energy Science (CEES), an Energy Frontier Research Center (EFRC) funded by the U.S. Department of Energy, Office of Science, Office of Basic Energy Sciences (Contract No. DE-AC02-06CH11357). The scanning electron microscopy studies were conducted at the Irving and Cherna Moskowitz Center for Nano and Bio-Nano Imaging at the Weizmann Institute of Science.

Notes and references

† *Department of Organic Chemistry, and ‡Department of Chemical Research Support, Weizmann Institute of Science, Rehovot 7610001, Israel. Email: milko.vanderboom@weizmann.ac.il*

§ *Department of Physics and Astronomy and Department of Materials Science and Engineering, Northwestern University, Evanston, Illinois 60208, USA.*

† Electronic Supplementary Information (ESI) available: Experimental procedures and characterization data. See DOI: 10.1039/b000000x/

1 R. Custelcean, *Chem. Soc. Rev.*, 2014, **43**, 1813-1824.
2 M. W. Hosseini, J.-M. Lehn, *Helv. Chim. Acta*, 1986, **69**, 587-603.
3 L. J. Kaplan, G. R. Weisman and D. J. Cram, *J. Org. Chem.*, 1979, **44**, 2226-2233.
4 I. A. Riddell, M. M. J. Smulders, J. K. Clegg, Y. R. Hristova, B. Breiner, J. D. Thoburn, J. R. Nitschke, *Nat. Chem*, 2012, **4**, 751-756.
5 I. Rubinstein, A. Vaskevich, *Israel J. Chem.*, 2010, **50**, 333-346.
6 H. E. Katz, *Chem. Mater.*, 1994, **6**, 2227-2232.
7 D. Zacher, R. Schmid, C. Wöll, R. A. Fischer, *Angew. Chem. Int. Ed.*, 2011, **50**, 176–199.

8 R. Balgley, S. Shankar, M. Lahav and M. E. van der Boom, *Angew. Chem. Int. Ed.*, 2015, **54**, 12457–12462.
9 Y. Nishimori, K. Kanaizuka, T. Kurita, T. Nagatsu, Y. Segawa, F. Toshimitsu, S. Muratsugu, M. Utsuno, S. Kume, M. Murata, H. Nishihara, *Chem. Asian J.*, 2009, **4**, 1361-1367.
10 N. Tuccitto, V. Ferri, M. Cavazzini, S. Quici, G. Zhavnerko, A. Licciardello and M. A. Rampi, *Nat. Mater*, 2009, **8**, 41-46.
11 J. Liu, T. Wächter, A. Irmler, P. G. Weidler, H. Gliemann, F. Pauly, V. Mugnaini, M. Zharnikov and C. Wöll, *ACS Appl. Mater. Inter.*, 2015, **7**, 9824-9830.
12 L. Motiei, M. Lahav, A. Gulino, M. A. Iron, M. E. van der Boom, *J. Phys. Chem. B*, 2010, **114**, 14283-14286.
13 S. Shankar, M. Lahav, M. E. van der Boom, *J. Am. Chem. Soc.*, 2015, **137**, 4050-4053.
14 M. Schott, W. Szczerba, D. G. Kurth, *Langmuir*, 2014, **30**, 10721-10727.
15 K. Takada, R. Sakamoto, S.-T. Yi, S. Katagiri, T. Kambe, H. Nishihara, *J. Am. Chem. Soc.*, 2015, **137**, 4681–4689.
16 L. Motiei, Y. Yao, J. Choudhury, H. Yan, T. J. Marks, M. E. van der Boom, A. Facchetti, *J. Am. Chem. Soc.*, 2010, **132**, 12528-12530.
17 P. C. Mondal, V. Singh, Y. L. Jeyachandran, M. Zharnikov, *ACS Appl. Mater. Inter.*, 2015, **7**, 8677-8686.
18 G. de Ruiter, M. E. van der Boom, *Acc. Chem. Res.*, 2011, **44**, 563-573.
19 V. Kaliginedi, H. Ozawa, A. Kuzume, S. Maharajan, I. V. Pobelov, N. H. Kwon, M. Mohos, P. Broekmann, K. M. Fromm, M.-A. Haga and T. Wandlowski, *Nanoscale*, 2015, DOI: 10.1039/C5NR04087F.
20 X. Li, X. Zhao, J. Zhang and Y. Zhao, *Chem. Commun.*, 2013, **49**, 10004-10006.
21 G. de Ruiter, M. Lahav and M. E. van der Boom, *Acc. Chem. Res.*, 2014, **47**, 3407-3416.
22 Y. Liang, R. H. Schmehl, *J. Chem. Soc., Chem. Commun.*, 1995, 1007-1008.
23 T. Heinrich, C. H.-H. Traulsen, M. Holzweber, S. Richter, V. Kunz, S. K. Kastner, S. O. Krabbenborg, J. Huskens, W. E. S. Unger and C. A. Schalley, *J. Am. Chem. Soc.*, 2015, **137**, 4382–4390.
24 J. Poppenberg, S. Richter, C. H. H. Traulsen, E. Darlatt, B. Baytekin, T. Heinrich, P. M. Deutinger, K. Huth, W. E. S. Unger and C. A. Schalley, *Chem. Sci.*, 2013, **4**, 3131-3139.
25 J. Choudhury, R. Kaminker, L. Motiei, G. d. Ruiter, M. Morozov, F. Lupo, A. Gulino and M. E. van der Boom, *J. Am. Chem. Soc.*, 2010, **132**, 9295-9297.
26 L. Motiei, M. Feller, G. Evmenenko, P. Dutta and M. E. van der Boom, *Chem. Sci.*, 2012, **3**, 66-71.
27 T. Shirman, R. Kaminker, D. Freeman and M. E. van der Boom, *ACS Nano*, 2011, **5**, 6553-6563.
28 A. A. Mamedov and N. A. Kotov, *Langmuir*, 2000, **16**, 5530-5533.
29 S. Kinge, M. Crego-Calama and D. N. Reinhoudt, *ChemPhysChem*, 2008, **9**, 20-42.
30 S. Prakash, T. Chakrabarty, A. K. Singh and V. K. Shahi, *Biosens. Bioelectron*, 2013, **41**, 43-53.
31 A. N. Shipway and I. Willner, *Chem. Commun.*, 2001, 2035-2045.
32 C. H.-H. Traulsen, V. Kunz, T. Heinrich, S. Richter, M. Holzweber, A. Schulz, L. K. S. von Krbek, U. T. J. Scheuschner, J. Poppenberg, W. E. S. Unger and C. A. Schalley, *Langmuir*, 2013, **29**, 14284–14292.
33 C. Sik Cho, K. Itotani and S. Uemura, *J. Organomet. Chem.*, 1993, **443**, 253-259.
34 L. Motiei, M. Sassi, R. Kaminker, G. Evmenenko, P. Dutta, M. A. Iron and M. E. van der Boom, *Langmuir*, 2011, **27**, 1319-1325.
35 G. Evmenenko, M. E. van der Boom, J. Kmetko, S. W. Dugan, T. J. Marks and P. Dutta, *J. Chem. Phys.*, 2001, **115**, 6722-6727.
36 T. Shinomiya, ., H. Ozawa, Y. Mutoh and M. Haga, *Dalton Trans.*, 2013, **42**, 16166-16175.
37 Naumkin A.V., K.-V. A., G. S.W. and P. C.J., *NIST Standard Reference Database 20, Version 4.1.*, 2012.
38 H. C. Brown, U. S. Racherla, *Tetrahedron Lett.*, 1985, **26**, 4311-4314.
39 M. R. Hansen, T. Vosegaard, H. J. Jakobsen and J. Skibsted, *J. Phys. Chem. A*, 2004, **108**, 586-594.
40 L. Motiei, R. Kaminker, M. Sassi, M. E. van der Boom, *J. Am. Chem. Soc.*, 2011, **133**, 14264-14266.